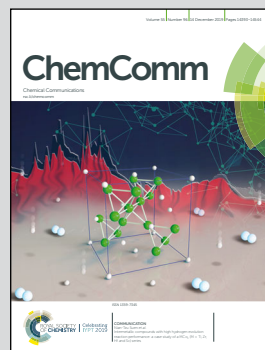


Showcasing research from Yu-Bin Dong's laboratory,  
Department of Chemistry, Shandong Normal University,  
Jinan, China.

A palladium–carbon-connected organometallic framework and  
its catalytic application

An organometallic framework (OMF) can be readily prepared *via* self-assembly of  $\text{PdI}_2$  and a divergent tridentate arylisocyanide ligand under solvothermal conditions. The obtained Pd–C bond connected 2D Pd-OMF can act as a highly active catalyst to promote the Suzuki–Miyaura cross-coupling reaction in a heterogeneous way.

As featured in:



See Yu-Bin Dong *et al.*,  
*Chem. Commun.*, 2019, **55**, 14414.



# A palladium–carbon-connected organometallic framework and its catalytic application†

Ying Dong,<sup>a</sup> Jing-Jing Jv,<sup>a</sup> Xiao-Wei Wu,<sup>ib</sup> Jing-Lan Kan,<sup>a</sup> Ting Lin<sup>a</sup> and Yu-Bin Dong<sup>ib</sup>\*<sup>a</sup>

Cite this: *Chem. Commun.*, 2019, 55, 14414

Received 5th October 2019,  
Accepted 17th October 2019

DOI: 10.1039/c9cc07829k

rsc.li/chemcomm

Herein, we report an organometallic framework (OMF) generated from a divergent tridentate arylisocyanide ligand and PdI<sub>2</sub> under solvothermal conditions. The obtained Pd–C bond-connected two-dimensional Pd-OMF was crystalline and porous. Moreover, it could be a highly active catalyst to promote the Suzuki–Miyaura cross-coupling reaction in a heterogeneous manner.

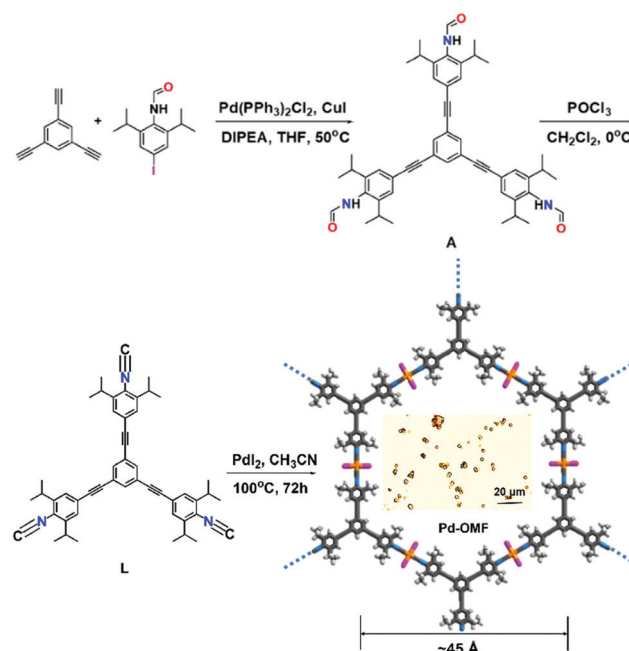
As two well-known types of porous polymeric materials, metal–organic frameworks (MOFs)<sup>1</sup> and covalent organic frameworks (COFs),<sup>2</sup> have been garnering intense attention due to their fascinating structures and potential applications in gas adsorption–separation,<sup>3</sup> catalysis,<sup>4</sup> medicine,<sup>5</sup> and sensing.<sup>6</sup>

By analogy with molecular chemistry,<sup>7</sup> metal–carbon (M–C) bond-driven polymeric porous species should also be present widely, but such species are rare.<sup>8</sup> Different from conventional metal–heteroatom-driven MOFs, organometallic frameworks (OMFs) are connected *via* metal–carbon linkages, although they are all driven by metal–ligand interaction. In doing so, the inherent functionalities shown by the porous polymeric materials derived from the inorganic, organometallic, and organic building blocks will be displayed fully.

Isocyanide is a typical organometallic coordination group that can bind various transition metal ions *via* strong  $\sigma$ -donating and weak  $\pi$ -back bonds, giving rise to various stable organometallic complexes.<sup>9</sup> It is similar to heteroatom ligands; isocyanide ligands can also accommodate most metal coordination geometries and, furthermore, propagate their geometry codes in a reversible way to form regular structures.

In this contribution, we report an OMF which is generated from a divergent tridentate arylisocyanide ligand **L** and PdI<sub>2</sub> under solvothermal conditions. The obtained Pd-OMF (Pd<sub>1.5</sub>I<sub>3</sub>L) featured an extended two-dimensional (2D) OMF network that was driven by the Pd–C bond. Furthermore, it could be a highly active catalyst to promote the Suzuki–Miyaura cross-coupling reaction under mild conditions in a heterogeneous manner.

As shown in Scheme 1, the tridentate arylisocyanide ligand **L** was prepared by POCl<sub>3</sub>-assisted dehydration of the triformamide intermediate **A** (ESI†). Upon mixing with PdI<sub>2</sub> in dry CH<sub>3</sub>CN, Pd-OMF was obtained as micro-sized light-yellow crystals under solvothermal conditions (100 °C, 72 h) in 76% yield (Scheme 1 and ESI†).



**Scheme 1** The synthesis of **L** and Pd-OMF. The Pd-OMF crystal structure generated using Materials Studio and a sample photograph are also shown.

<sup>a</sup> College of Chemistry, Chemical Engineering and Materials Science, Collaborative Innovation Centre of Functionalized Probes for Chemical Imaging in Universities of Shandong, Key Laboratory of Molecular and Nano Probes, Ministry of Education, Shandong Normal University, Jinan 250014, P. R. China. E-mail: yubindong@sdsu.edu.cn

<sup>b</sup> School of Chemical Engineering, Nanjing University of Science and Technology, Nanjing, Jiangsu 210094, P. R. China

† Electronic supplementary information (ESI) available: The synthesis and additional characterization of **L** and Pd-OMF; catalytic procedures, GC analysis, the proposed mechanism, and crystallographic information for Pd-OMF. See DOI: 10.1039/c9cc07829k



As indicated in the infrared (IR) spectra (Fig. 1a), the characteristic sharp peak of  $\text{-N}\equiv\text{C}$  at  $2110\text{ cm}^{-1}$  in **L** moved to  $2183\text{ cm}^{-1}$  after reaction with  $\text{PdI}_2$ , indicating that the isocyanide donors coordinated with  $\text{Pd(II)}$  and the Pd-C-bonded **Pd-OMF** was formed.<sup>10</sup> Evidence that **Pd-OMF** had been formed was further supported by  $^{13}\text{C}$  cross-polarization magic-angle spinning (CP/MAS) nuclear magnetic resonance (NMR) spectroscopy. As shown in Fig. 1b, the peaks associated with the aliphatic carbons of  $\text{-CH}_3$  and  $\text{-CH(CH}_3)_2$  groups were located at 25.4 and 31.1 ppm, respectively. The signal at 170.4 ppm in **L** assignable to  $\text{-N}\equiv\text{C}$  carbon was upfield-shifted to 120.1 ppm as a shoulder peak in **Pd-OMF**.<sup>10</sup> This spectroscopic change corroborated well with formation of the Pd-C bond. Besides, the broad low-intensity peak at  $\sim 92.4$  ppm was ascribed to acetylene carbons, and the broad signals at *ca.* 126.4, 136.0, 144.9 and 148.3 ppm were assigned unambiguously to aromatic carbons.

The oxidation state of the Pd species in **Pd-OMF** was determined by X-ray photoelectron spectroscopy (XPS). As shown in Fig. 1c, the binding energies for Pd  $3d_{5/2}$  and  $3d_{3/2}$  were 338.0 and 343.1 eV respectively, suggesting that the Pd valence in **Pd-OMF** was bivalent.<sup>11</sup> Elemental analysis confirmed the formation of **Pd-OMF** with a formula of  $(\text{C}_{51}\text{H}_{54}\text{I}_3\text{N}_3\text{Pd}_{1.5})_n$  (ESI<sup>†</sup>). In addition, inductively coupled plasma (ICP) analyses showed that the Pd content in **Pd-OMF** was 12.46 wt% (calcd 12.78 wt% based on  $\text{C}_{51}\text{H}_{54}\text{I}_3\text{N}_3\text{Pd}_{1.5}$ ).

Scanning electron microscopy (SEM) showed that the as-synthesized sample featured lamellar morphology (ESI<sup>†</sup>). SEM-energy dispersive X-ray (EDX) mapping showed that the C, N, I and Pd were distributed evenly in the OMF matrix (ESI<sup>†</sup>). Notably, attempts have been made by varying the synthetic conditions (including different reaction temperatures, solvents, and metal: ligand ratio) to grow single crystals of **Pd-OMF** of suitable size for X-ray single-crystal analyses, but they have all failed. As indicated in Scheme 1, the obtained crystals were too small to be used for X-ray single-crystal analyses. Thermogravimetric analysis (TGA)

of **Pd-OMF** showed no obvious weight loss  $\leq 350^\circ\text{C}$  in air, indicating its good thermal stability (ESI<sup>†</sup>).

Alternatively, structural modeling has been carried out with Materials Studio v2018.<sup>12</sup> The crystal structure of **Pd-OMF** was established based on powder X-ray diffraction (PXRD) data with Cu  $K\alpha$  radiation. As shown in Fig. 2, **Pd-OMF** was highly crystalline, and displayed prominent diffraction peaks at  $2.3^\circ$ ,  $4.7^\circ$ ,  $6.0^\circ$ ,  $6.9^\circ$ ,  $7.9^\circ$ ,  $8.7^\circ$ , and  $9.6^\circ$  in its PXRD pattern, which could be assigned to (100), (200), (210), (310), (101), (201), and (211) facets, respectively (Fig. 2, black curve). The obtained PXRD pattern from **Pd-OMF** was completely different from its **L** and  $\text{PdI}_2$  precursors (ESI<sup>†</sup>), implying the formation of new crystalline species. To elucidate the structure of **Pd-OMF** and to calculate the unit-cell parameters, two types of possible 2D structures were generated. That is, eclipsed (AA) (Fig. 2a) and staggered stacking (AB) models (Fig. 2b) were built and optimized by the Forcite molecular dynamics module within Materials Studio. Different from the AA stacking model, the experimental PXRD pattern for **Pd-OMF** matched well with the simulated pattern of the staggered stacking (AB) model in the hexagonal  $P6_3/mmc$  space group. Pawley refinement showed a negligible difference between the simulated PXRD pattern and experimental patterns, and gave the optimized parameters  $a = b = 44.6\text{ \AA}$ ,  $c = 11.8\text{ \AA}$ ,  $\alpha = \beta = 90^\circ$ , and  $\gamma = 120^\circ$  (residuals  $R_{wp} = 4.52\%$  and  $R_p = 3.17\%$ , ESI<sup>†</sup>).

Structural analyses revealed that the  $\text{PdI}_2$  in **Pd-OMF** was linked together by **L** via a *trans*-diiodobis(isocyanide)-Pd linkage into a 2D OMF net extended in the crystallographic *ab* plane with a honeycomb-like cavity in which the opposite Pd...Pd distance was  $\sim 45\text{ \AA}$  (Scheme 1). As shown in Fig. 2b,

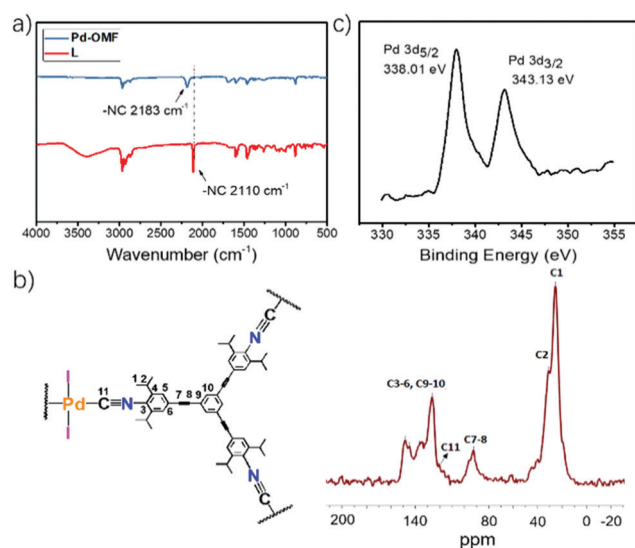


Fig. 1 (a) IR spectra of **L** and **Pd-OMF**. (b) The  $^{13}\text{C}$  NMR spectrum of **Pd-OMF**. (c) The XPS spectrum for Pd species in **Pd-OMF**.

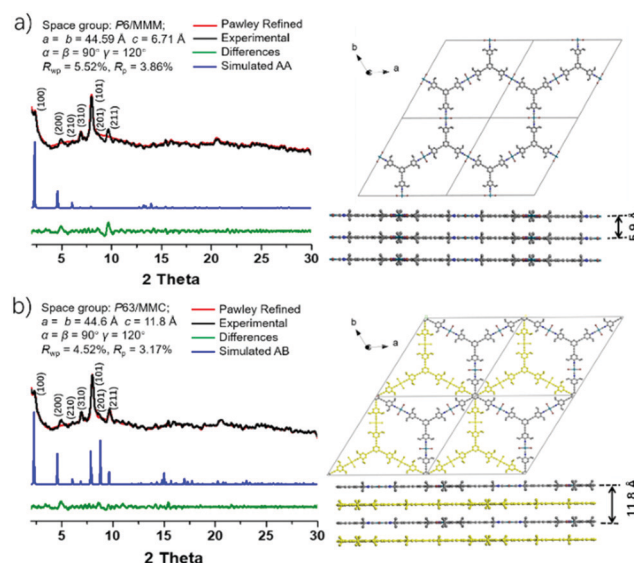


Fig. 2 The PXRD patterns of **Pd-OMF**: a comparison between the experimental (black curves) and Pawley-refined (red curves) profiles, simulated patterns for AA (a) and AB (b) stacking modes (blue curves) and refinement differences (green curves). The insets are structural models of **Pd-OMF** with AA (a) and AB (b) stacking styles. For the staggered structure, alternating yellow layers with undefined atoms are presented for better visibility.

structural AB-modeling revealed that these 2D nets stacked together along the crystallographic *c* axis in an AB-fashion to generate rhombic channels with a reduced pore size (opposite Pd...Pd distance at  $\sim 28$  Å) due to their staggered arrangement.

Transmission electron microscopy (TEM) also showed **Pd-OMF** possessing a 2D layered structure with an interlayer distance of 5.9 Å (ESI<sup>†</sup>), which was consistent with its structural modeling.

N<sub>2</sub> sorption undertaken at 77 K provided a Brunauer–Emmett–Teller (BET) surface area of 205.80 m<sup>2</sup> g<sup>−1</sup> for **Pd-OMF**. The observed type-IV isotherm was indicative of its mesoporous characteristics. Pore-size distribution based on nonlocal density functional theory (NLDFT) was done. It revealed that **Pd-OMF** displayed a pore-size-distribution centered at  $\sim 19 \pm 1$  Å, which was in good agreement with its simulated structure (ESI<sup>†</sup>).

Molecular isocyanide–Pd complexes have been reported to be a highly efficient class of catalyst in various C–C coupling reactions, but in a homogeneous way.<sup>13</sup> By means of an OMF platform, the isocyanide–Pd species herein was loaded and fixed in an orderly manner within the polymeric OMF. Therefore, its heterogeneous catalysis for recyclable C–C coupling should be feasible.

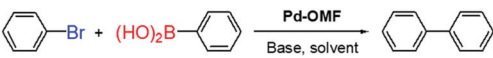
The catalytic activity of **Pd-OMF** for the Suzuki–Miyaura cross-coupling reaction was examined, in which the coupling between bromobenzene and phenylboronic acid was chosen as the model reaction. As shown in Table 1, solvent screening revealed MeOH to be the best solvent among toluene, THF, dioxane, DMF, isopropyl alcohol (IPA), acetone, and MeCN (Table 1, entries 1–8). In addition, the bases K<sub>2</sub>CO<sub>3</sub>, K<sub>3</sub>PO<sub>4</sub>, Na<sub>2</sub>CO<sub>3</sub>, KOH, triethylamine (TEA), and 1,8-diazabicyclo[5.4.0]undec-7-ene (DBU), were used to carry

out the reaction. K<sub>2</sub>CO<sub>3</sub> was better than the other inorganic and organic bases (Table 1, entries 8–13). Furthermore, when the reaction was carried out with less catalyst loading, 0.1 (Table 1, entry 14) or 0.5 (Table 1, entry 15) instead of 0.7 mol%, the coupled product was obtained at lower (75% and 93%) yields. Conversely, the reaction temperature appeared to be crucial for catalytic efficiency. As indicated in Table 1, the catalytic activity of **Pd-OMF** was largely diminished at lower temperature (Table 1, entries 16 and 17). In addition, shortening the reaction time led to reduced (75–86%) yields under the given conditions (Table 1, entries 18 and 19). We did not observe any desired product in the absence of **Pd-OMF** even at 70 °C at 8 h (Table 1, entry 20). Based on these observations, the optimal conditions for the model cross-coupling reaction were set as 0.7 mol% of Pd, K<sub>2</sub>CO<sub>3</sub> (base), MeOH (solvent), 70 °C, and 8 h (reaction time) (Table 1, entry 8).

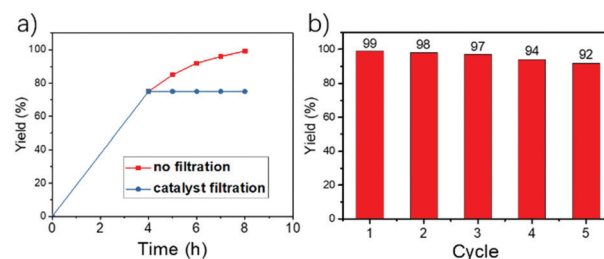
As shown in Fig. 3a, no further reaction occurred after ignition of the reaction at 4.0 h when it reached  $\sim 75\%$  yield. Gas chromatography (GC) monitoring indicated that the yield was unaltered during the prolonged reaction time. This suggested that **Pd-OMF** was a typical heterogeneous catalyst and, as such, it could be reused, and its catalytic yield was  $\leq 92\%$  after five runs (Fig. 3b and ESI<sup>†</sup>). After multiple catalytic cycles, no valence change of the Pd species was detected based on the XPS spectrum (ESI<sup>†</sup>). Inductively coupled plasma (ICP) analyses showed that the Pd amount in **Pd-OMF** was 12.33 wt%, suggesting that only  $\sim 1$  wt% Pd leached after five runs. Hence, the arylisocyanide is an ideal class of organic ligand that can firmly bind Pd(II) ions *via* M–C bonds and, furthermore, incorporate them into the extended OMFs. The measured PXRD pattern, SEM, and energy-dispersive X-ray-SEM spectra demonstrated that the structural integrity, crystallinity, morphology, and uniform elemental distribution of **Pd-OMF** were well maintained after multiple catalytic use (ESI<sup>†</sup>).

Notably, **Pd-OMF** was tolerant to a wide range of substrates with different functional groups (–NO<sub>2</sub>, –COCH<sub>3</sub>, –OCH<sub>3</sub>, –OH, –CH<sub>3</sub>, –CO<sub>2</sub>Me, –CN) at different substituted positions. As shown in Table 2, phenyl bromides with electron-donating and electron-withdrawing groups afforded cross-coupling products with excellent yields (97–99%, entries 1–9). Compared with phenyl bromides, phenyl iodides were more active. For example, the coupling yield

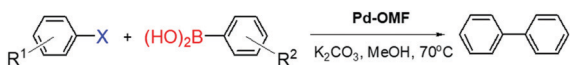
**Table 1** Optimization of the model Suzuki–Miyaura coupling reaction between bromobenzene and phenylboronic acid<sup>a</sup>

|  |           |                                 |         |               |              |                        |
|---|-----------|---------------------------------|---------|---------------|--------------|------------------------|
| Entry   | Pd (mol%) | Base                            | Sol.    | <i>T</i> (°C) | <i>t</i> (h) | Yield <sup>b</sup> (%) |
| 1   | 0.7       | K <sub>2</sub> CO <sub>3</sub>  | Toluene | 70            | 8            | 75                     |
| 2   | 0.7       | K <sub>2</sub> CO <sub>3</sub>  | THF     | 70            | 8            | 65                     |
| 3   | 0.7       | K <sub>2</sub> CO <sub>3</sub>  | Dioxane | 70            | 8            | 20                     |
| 4   | 0.7       | K <sub>2</sub> CO <sub>3</sub>  | DMF     | 70            | 8            | 86                     |
| 5   | 0.7       | K <sub>2</sub> CO <sub>3</sub>  | IPA     | 70            | 8            | 83                     |
| 6   | 0.7       | K <sub>2</sub> CO <sub>3</sub>  | Acetone | 70            | 8            | 23                     |
| 7   | 0.7       | K <sub>2</sub> CO <sub>3</sub>  | MeCN    | 70            | 8            | 24                     |
| 8   | 0.7       | K <sub>2</sub> CO <sub>3</sub>  | MeOH    | 70            | 8            | > 99                   |
| 9   | 0.7       | K <sub>3</sub> PO <sub>4</sub>  | MeOH    | 70            | 8            | 97                     |
| 10  | 0.7       | Na <sub>2</sub> CO <sub>3</sub> | MeOH    | 70            | 8            | 95                     |
| 11  | 0.7       | KOH                             | MeOH    | 70            | 8            | 94                     |
| 12  | 0.7       | TEA                             | MeOH    | 70            | 8            | 33                     |
| 13  | 0.7       | DBU                             | MeOH    | 70            | 8            | 23                     |
| 14  | 0.1       | K <sub>2</sub> CO <sub>3</sub>  | MeOH    | 70            | 8            | 64                     |
| 15  | 0.5       | K <sub>2</sub> CO <sub>3</sub>  | MeOH    | 70            | 8            | 93                     |
| 16  | 0.7       | K <sub>2</sub> CO <sub>3</sub>  | MeOH    | rt            | 8            | 43                     |
| 17  | 0.7       | K <sub>2</sub> CO <sub>3</sub>  | MeOH    | 50            | 8            | 83                     |
| 18  | 0.7       | K <sub>2</sub> CO <sub>3</sub>  | MeOH    | 70            | 4            | 75                     |
| 19  | 0.7       | K <sub>2</sub> CO <sub>3</sub>  | MeOH    | 70            | 6            | 86                     |
| 20  | —         | K <sub>2</sub> CO <sub>3</sub>  | MeOH    | 70            | 8            | —                      |

<sup>a</sup> Reaction conditions: bromobenzene (1.0 mmol), phenylboronic acid (1.1 mmol), base (2.0 mmol), solvent (2 mL), in N<sub>2</sub>. <sup>b</sup> Yields were determined by gas chromatography (ESI).



**Fig. 3** (a) Leaching test for the model Suzuki–Miyaura cross-coupling reaction. (b) Yields of diphenyl over repeated runs for the model Suzuki–Miyaura cross-coupling reaction. After each run, **Pd-OMF** was recollected *via* centrifugation, washed with MeCN (3 × 2 mL) and CHCl<sub>3</sub> (3 × 2 mL), and dried at 110 °C for 24 h under vacuum, and then reused for the next catalytic run under identical reaction conditions.

**Table 2** Cross-coupling reactions of various PhX and PhB(OH)<sub>2</sub> molecules catalyzed by **Pd-OMF**<sup>a</sup>


| Entry          | R <sup>1</sup>                    | X  | R <sup>2</sup>     | t (h) | Yield <sup>b</sup> (%) |
|----------------|-----------------------------------|----|--------------------|-------|------------------------|
| 1              | H                                 | Br | H                  | 8     | 99                     |
| 2              | 4-NO <sub>2</sub>                 | Br | H                  | 8     | 99                     |
| 3 <sup>c</sup> | 4-COCH <sub>3</sub>               | Br | H                  | 8     | 99                     |
| 4              | 4-OCH <sub>3</sub>                | Br | H                  | 8     | 99                     |
| 5              | 3-OH                              | Br | H                  | 8     | 99                     |
| 6              | 2-CN                              | Br | H                  | 8     | 97                     |
| 7              | 2-CH <sub>3</sub>                 | Br | H                  | 8     | 99                     |
| 8              | 3-NO <sub>2</sub>                 | Br | H                  | 8     | 99                     |
| 9              | H                                 | Br | 4-OCH <sub>3</sub> | 8     | 99                     |
| 10             | H                                 | I  | H                  | 7     | 99                     |
| 11             | 2-OCH <sub>3</sub>                | I  | H                  | 7     | 99                     |
| 12             | 2-CF <sub>3</sub>                 | I  | H                  | 7     | 99                     |
| 13             | 3-CH <sub>3</sub>                 | I  | H                  | 7     | 99                     |
| 14             | 3-NO <sub>2</sub>                 | I  | H                  | 7     | 99                     |
| 15             | 4-OCH <sub>3</sub>                | I  | H                  | 7     | 99                     |
| 16             | 4-CN                              | I  | H                  | 7     | 99                     |
| 17             | 4-CO <sub>2</sub> CH <sub>3</sub> | I  | H                  | 7     | 99                     |
| 18             | H                                 | I  | 2-OCH <sub>3</sub> | 8     | 99                     |
| 19             | 3-NO <sub>2</sub>                 | I  | 4-F                | 8     | >99                    |
| 20             | 4-CN                              | I  | 3-OCH <sub>3</sub> | 8     | >99                    |
| 21             | H                                 | I  | 4-CN               | 8     | 96                     |
| 22             | H                                 | Cl | H                  | 8     | 6                      |
| 23             | 4-CF <sub>3</sub>                 | Cl | H                  | 8     | 9                      |
| 24             | 4-NO <sub>2</sub>                 | Cl | H                  | 8     | 55                     |
| 25             | 2-CN                              | Cl | H                  | 8     | 45                     |

<sup>a</sup> Reaction conditions: PhX (1.0 mmol), PhB(OH)<sub>2</sub> (1.1 mmol), K<sub>2</sub>CO<sub>3</sub> (2 mmol, 0.276 g), **Pd-OMF** (0.7 mol% Pd equiv.), methanol (2 mL), 70 °C, in N<sub>2</sub>. <sup>b</sup> Yields were determined by GC (ESI). <sup>c</sup> 4'-Bromoacetophenone and phenylboronic acid coupling gave 76% yield in the presence of molecular (AdNC)<sub>2</sub>PdCl<sub>2</sub> catalyst (PhX, 1 mmol; PhB(OH)<sub>2</sub>, 1.2 mmol; Cs<sub>2</sub>CO<sub>3</sub>, 2.2 mmol; (AdNC)<sub>2</sub>PdCl<sub>2</sub>, 0.05 mmol; refluxed in dioxane for 18 h).<sup>14</sup>

based on iodobenzene and 2-, 4- or 3-substituted phenyl iodides was 99% even at 7 h (Table 2, entries 10–17). For coupling with substituted phenylboronic acids, phenyl iodides also afforded excellent yields of 96% to >99% but in 8 h (Table 2, entries 18–21).

In contrast, **Pd-OMF** could not effectively activate ArCl-based Suzuki–Miyaura reactions. For example, the coupling of phenylboronic acid with chlorobenzene or trifluoromethylchlorobenzene only gave 6% or 9% yield under given conditions (Table 2, entries 22 and 23). The coupling of nitro- or cyano-substituted phenyl chlorine with phenylboronic acid, however, provided moderate (55% or 45%) yields (Table 2, entries 24 and 25).

The possible mechanism of the **Pd-OMF**-catalysed Suzuki–Miyaura coupling reaction was believed to be the same as that of molecular isocyanide–Pd-promoted coupling reactions in solution (ESI<sup>†</sup>).<sup>13</sup> In comparison with molecular isocyanide–Pd catalysts, **Pd-OMF** required less catalyst-loading, a lower reaction temperature, and shorter reaction time, but elicited a much higher reaction yield (Table 2, footnote for entry 3).

In summary, we prepared a Pd–C bond-connected OMF and, furthermore, introduced the Pd–isocyanide species into an OMF network. The obtained **Pd-OMF** exhibited high catalytic activity to promote the Suzuki–Miyaura cross-coupling reaction in a heterogeneous way. We have expanded the research field of polymeric porous materials driven by metal–carbon bonding interactions.

We are grateful for financial support from NSFC (21971153, 21671122, 21802091), Taishan Scholar's Construction Project, and Changjiang Scholar Project at SDNU.

## Conflicts of interest

There are no conflicts of interest to declare.

## Notes and references

- H.-C. Zhou, J. R. Long and O. M. Yaghi, *Chem. Rev.*, 2012, **112**, 673–674.
- (a) P. J. Waller, F. Gandara and O. M. Yaghi, *Acc. Chem. Res.*, 2015, **48**, 3053–3063; (b) X. Feng, X. Ding and D. Jiang, *Chem. Soc. Rev.*, 2012, **41**, 6010–6022.
- (a) J.-R. Li, J. Sculley and H.-C. Zhou, *Chem. Rev.*, 2012, **112**, 869–932; (b) S. Yuan, X. Li, J. Zhu, G. Zhang, P. V. Puyvelde and B. V. der Bruggen, *Chem. Soc. Rev.*, 2019, **48**, 2665–2681.
- (a) M. Yoon, R. Srirambalaji and K. Kim, *Chem. Rev.*, 2012, **112**, 1196–1231; (b) S.-Y. Ding and W. Wang, *Chem. Soc. Rev.*, 2013, **42**, 548–568.
- (a) P. Horcajada, R. Gref, T. Baati, P. K. Allan, G. Maurin, P. Couvreur, G. Férey, R. E. Morris and C. Serre, *Chem. Rev.*, 2012, **112**, 1232–1268; (b) Q. Guan, Y.-A. Li, W.-Y. Li and Y.-B. Dong, *Chem. – Asian J.*, 2018, **13**, 3122–3149; (c) Q. Guan, D.-D. Fu, Y.-A. Li, X.-M. Kong, Z.-Y. Wei, W.-Y. Li, S.-J. Zhang and Y.-B. Dong, *iScience*, 2019, **14**, 180–198.
- (a) L. E. Kreno, K. Leong, O. K. Farha, M. Allendorf, R. P. Van Duyne and J. T. Hupp, *Chem. Rev.*, 2012, **112**, 1105–1125; (b) X. Liu, D. Huang, C. Lai, G. Zeng, L. Qin, H. Wang, H. Yi, B. Li, S. Liu, M. Zhang, R. Deng, Y. Fu, L. Li, W. Xue and S. Chen, *Chem. Soc. Rev.*, 2019, **48**, 5266–5302.
- J. D. Dunitz and L. E. Orgen, *Nature*, 1953, **171**, 121–122.
- Although metal–carbon bond can be used to connect extended organometallic structures in principle, only few such examples have been reported thus far: (a) D. W. Agnew, I. M. DiMucci, A. Arroyave, M. Gembicky, C. E. Moore, S. N. MacMillan, A. L. Rheingold, K. M. Lancaster and J. S. Figueroa, *J. Am. Chem. Soc.*, 2017, **139**, 17257–17260; (b) D. W. Agnew, M. Gembicky, C. E. Moore, A. L. Rheingold and J. S. Figueroa, *J. Am. Chem. Soc.*, 2016, **138**, 15138–15141.
- (a) E. Hahn, *Angew. Chem., Int. Ed., Engl.*, 1993, **32**, 650–665; (b) R. A. Michelin, A. J. L. Pombeiro, M. Fátima and C. G. da Silva, *Coord. Chem. Rev.*, 2001, **218**, 43–74; (c) B. R. Barnett and J. S. Figueroa, *Chem. Commun.*, 2016, **52**, 13829–13839.
- (a) A. Mayr and J. Guo, *Inorg. Chem.*, 1999, **38**, 921–928; (b) A. Mayr and L. F. Mao, *Inorg. Chem.*, 1998, **37**, 5776–5780.
- A. C. Thomas, *Photoelectron and Auger Spectroscopy*, Plenum, New York, 1975.
- Materials Studio Release Notes ver. 2018, Accelrys Software.
- K. T. Mahmudov, V. Y. Kukushkin, A. V. Gurbanov, M. A. Kinzhalov, V. P. Boyarskiy, M. F. C. G. da Silva and A. J. L. Pombeiro, *Coord. Chem. Rev.*, 2019, **384**, 65–89.
- D. Villemain, A. Jullien and N. Bar, *Tetrahedron Lett.*, 2007, **48**, 4191–4193.